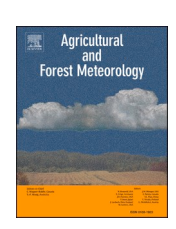
ELSEVIER

Contents lists available at ScienceDirect

Agricultural and Forest Meteorology

journal homepage: www.elsevier.com/locate/agrformet





Excluding quartz content from the estimation of saturated soil thermal conductivity: Combined use of differential effective medium theory and geometric mean method

Yongwei Fu^a, Scott Jones^b, Robert Horton^c, Joshua Heitman^{a,*}

- ^a Department of Crop & Soil Sciences, North Carolina State University, Raleigh 27695, United States
- b Department of Plants, Soils and Climate, Utah State University, Logan, UT 84322, United States
- ^c Department of Agronomy, Iowa State University, Ames 50011, United States

ARTICLE INFO

Keywords: Thermal conductivity Geometric mean method Differential effective medium theory Saturation

ABSTRACT

Saturated soil thermal conductivity (λ_{sat}) is the maximum soil thermal conductivity value of a given soil. Although it can be determined accurately with a heat pulse sensor, there are challenges to prepare fully saturated soil samples. Numerous models have been developed to estimate λ_{sat} , and among these, the geometric mean method (GMM) generally performs well. The GMM requires soil mineral composition or quartz content information, which is unavailable for most soils. Earlier studies commonly used assumed that quartz content (fquartz) was equal to sand content (f_{sand}) or to 0.5 × f_{sand} , which led to significant λ_{sat} estimation errors especially on coarse-textured soils. We derived a novel method to estimate λ_{sat} from soil porosity (ϕ) based on a combination of the GMM and differential effective medium theory (DEM). The new DEM-GMM approach has a single parameter, cementation exponent (m). Using a calibration dataset of 43 soils, we determined best fit m values for soils in three groups: 1.66 for Group I (f_{sand} < 0.4), 1.62 for Group II (0.4 <= f_{sand} < 1) and m = -1.34 ϕ +1.70 for Group III ($f_{\text{sand}} = 1$). Using best fit m values for different groups, the new model can estimate λ_{sat} values from ϕ . Independent validation results on another 46 soils showed that the new model outperformed the GMM method with the assumption that $f_{quartz} = f_{sand}$ or $f_{quartz} = 0.5 \times f_{sand}$. The mean RMSE, Bias and R² values of the DEM-GMM approach were 0.202 W m⁻¹ K⁻¹, 0.013 W m⁻¹ K⁻¹ and 0.89, respectively, and corresponding values of the GMM with the two assumptions were 0.295 and 0.476 W m⁻¹ K⁻¹, 0.056 and -0.28 W m⁻¹ K⁻¹, 0.80 and 0.82, respectively. The robust performance of the DEM-GMM approach suggests that it can be incorporated into thermal conductivity models to accurately estimate the thermal conductivity of unsaturated soils.

1. Introduction

Soil thermal conductivity (λ) is directly related to a soil's capability to conduct heat (Bristow, 2002). As soil is a three-phase system, soil λ is influenced by the thermal conductivity and volume fraction of each phase (e.g., porosity (ϕ) and water content (θ)). Thermal conductivity of soil solids (λ_s) is much greater than that of the other two phases (water and air) and water has a much larger thermal conductivity than does air. For a given soil, the magnitude of soil λ depends largely on θ and varies from dry to saturated states (de Vries, 1963). Dry soils can be regarded as a mixture of solid and air having relatively low thermal conductivity (λ_{dry}); in contrast, water-saturated soils have their highest value of thermal conductivity (λ_{sat}). There are many $\lambda(\theta)$ models available to estimate the thermal conductivity of unsaturated soils. Most of the

models require λ_{dry} and λ_{sat} as inputs, particularly the normalized thermal conductivity models, which were first proposed by Johansen (1975) and later included in many empirical models (Côté and Konrad, 2007; Lu et al., 2007; He et al., 2017). They can be written in a general form as follows:

$$\lambda = \lambda_{\text{sat}} K_{\text{e}} + \lambda_{\text{drv}} (1 - K_{\text{e}}) \tag{1}$$

where K_e is the Kersten coefficient as a function of θ . Thus, the effect of uncertainty in λ_{dry} and λ_{sat} estimates on the $\lambda(\theta)$ curve over the entire range of saturation ($0 \le \theta \le \phi$) are expressed as:

$$\delta \lambda = \delta \lambda_{\text{sat}} \int_0^{\phi} K_{\text{e}} d\theta \tag{2a}$$

^{*} Corresponding author.

E-mail address: jlheitman@ncsu.edu (J. Heitman).

Notation		Greek le	Greek letters				
		λ	thermal conductivity, W m^{-1} K $^{-1}$				
а	semi-major axial dimension, m	λ_{dry}	thermal conductivity of dry soils, W m^{-1} K $^{-1}$				
b	semi-minor axial dimension, m	λ_i	thermal conductivity of the $j_{\rm th}$ phase, W m $^{-1}$ K $^{-1}$				
c	semi-minor axial dimension, m	$\lambda_{\mathbf{k}}$	thermal conductivity at step k , W m ⁻¹ K ⁻¹				
D	effective depolarization factor, unitless	λ_{0}	thermal conductivity of other minerals, W m^{-1} K $^{-1}$				
D^a	depolarization factor at the semi-major axis, unitless	$\lambda_{\mathbf{q}}$	thermal conductivity of quartz, W m^{-1} K ⁻¹				
D^b	depolarization factor at the semi-minor axis, unitless	$\lambda_{\mathbf{s}}$	thermal conductivity of solids, W m ⁻¹ K ⁻¹				
D^c	depolarization factor at the semi-minor axis, unitless	λ_{sat}	saturated thermal conductivity, W $\mathrm{m}^{-1}~\mathrm{K}^{-1}$				
D^i	depolarization factor at i_{th} direction, unitless	λi sat	saturated thermal conductivity at i_{th} direction, W m ⁻¹ K ⁻¹				
F	electrical formation factor, unitless	$\lambda_{\mathbf{w}}$	thermal conductivity of water, W m ⁻¹ K ⁻¹				
f_j	volume fraction of the j_{th} phase, cm ³ cm ⁻³	$\lambda_{\mathbf{w}}^*$	relative thermal conductivity of water, W m ⁻¹ K ⁻¹				
$f_{ m quartz}$	quartz content, cm ³ cm ⁻³	$\sigma_{\rm s}$	electrical conductivities of solid particles, S m ⁻¹				
$f_{\rm sand}$	sand content, g g ⁻¹	σ_{sat}	saturated electrical conductivities, S m ⁻¹				
K_{e}	Kersten coefficient, unitless	$\sigma_{ m w}$	electrical conductivities of water, S m ⁻¹				
m	cementation exponent, unitless	θ	water content, cm ³ cm ⁻³				
T^*	relative temperature, K	ф	porosity, cm ³ cm ⁻³				
$V_{ m w}$	Volume of water, cm ³	ά	soil texture dependent parameter, unitless				
$V_{\rm s}$	Volume of solids, cm ³						

$$\delta \lambda = \delta \lambda_{\rm dry} \int_0^{\phi} (1 - K_{\rm e}) d\theta = \delta \lambda_{\rm dry} \left(\phi - \int_0^{\phi} K_{\rm e} d\theta \right)$$
 (2b)

where $\delta\lambda$, $\delta\lambda_{dry}$ and $\delta\lambda_{sat}$ represent the uncertainties in estimating the thermal conductivity values of unsaturated soils, dry soils and water-

saturated soils, respectively. Because the $\lambda(\theta)$ curve is sigmoidal,

 $K_{\rm c} {\rm d} \theta$ is always greater than $\phi/2$ (e.g., Fig. 1 in Lu et al. (2007)). Also, because $\lambda_{\rm sat}$ is much greater than $\lambda_{\rm dry}$, Eq. (2a) is expected to influence the $\lambda(\theta)$ curve much more than $\lambda_{\rm dry}$. Therefore, it is critical to accurately determine or estimate $\lambda_{\rm sat}$ for soil heat conduction calculations.

Benefiting from progress in measurement techniques (e.g., heat pulse method), λ_{sat} can generally be accurately determined (Bristow, 1998; He et al., 2018; Dixon et al., 2023). However, the preparation of saturated soil samples, particularly for fine-textured soils, poses serious problems caused by the difficulty of removing entrapped air, and due to soil swelling (Tarnawski et al., 2009). Therefore, it is unsurprising that many of the published $\lambda(\theta)$ datasets do not have measurements at or near saturated conditions. Consequently, there are numerous thermal conductivity models available in the literature to estimate λ_{sat} (Tarnawski

et al., 2018; Wang et al., 2020). They can generally be categorized into three types: theoretical models; semi-empirical models; and empirical models. Wang et al. (2020) reviewed a total of 52 models that estimate λ_{sat} , and they reported that none of the empirical models were accurate. The geometric mean method (GMM) performed the best, followed by seven theoretical models which all required thermal conductivity of soil solids λ_s as an input parameter. However, λ_s cannot be directly determined as "soil is a porous medium and there is no way to compact the soil to a continuous solid state without any pore spaces." Thus, λ_s values are not known for most soils (He et al., 2020b).

He et al. (2020b) summarized three types of approaches to estimate λ_s : (1) inverse estimation from λ_{sat} using the GMM; (2) empirical estimation using texture and porosity; (3) fitting models to saturation-dependent thermal conductivity ($\lambda(\theta)$) measurements, which treats λ_s as a model fitting parameter. Among the three approaches, the third type provides the best estimates of λ_s (Côté and Konrad, 2007; He et al., 2020b), but there are some limitations. First, model fitting results depend on the number and range of fitted $\lambda(\theta)$ datapoints, particularly in the range near saturation. Côté and Konrad (2007) reported that when using a single $\lambda(\theta)$ measurement, the Côté and Konrad (2005) model estimated λ_s values from 4.92 to 5.67 W m⁻¹ K⁻¹, whereas the estimated

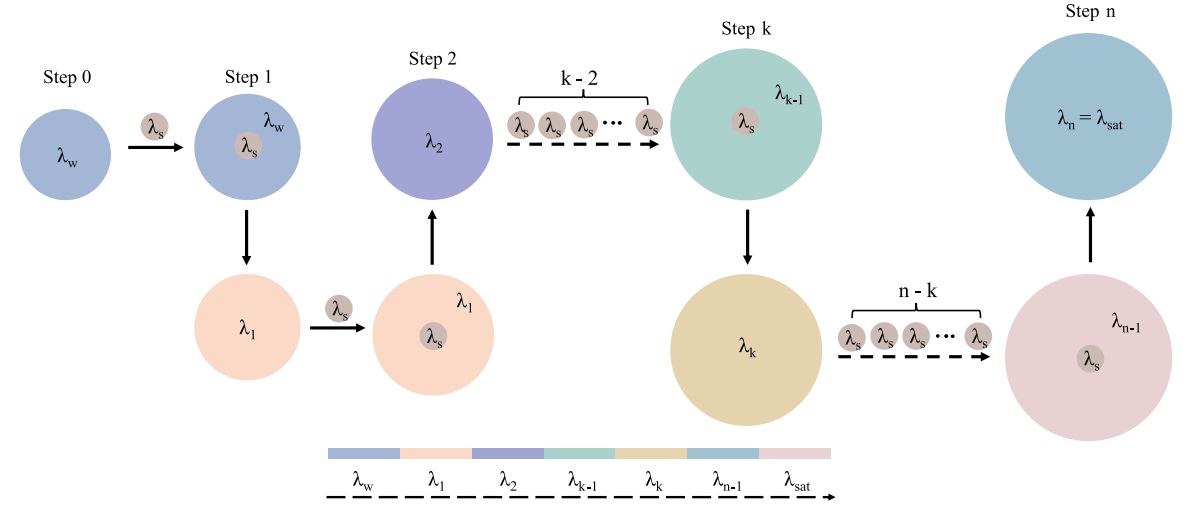


Fig. 1. The iterative process of the DEM theory.

 λ_s value was 5.08 W m $^{-1}$ K $^{-1}$ when five $\lambda(\theta)$ values were used. Model fitting results are also influenced by the robustness of the selected fitting equation. Lu et al. (2007) reported that Côté and Konrad (2005) model could not well capture the trend of $\lambda(\theta)$ curves at low and intermediate θ ranges as its hyperbolic form. Thus, if one uses $\lambda(\theta)$ datapoints at low and medium saturation to estimate λ_s , errors from the Côté and Konrad (2005) model itself are included in the λ_s estimations. For example, Côté and Konrad (2007) found the largest RMSE of λ_s for a crushed rock inversely estimated with the Côté and Konrad (2005) model, when $\lambda(\theta)$ datapoint at $\theta=0.009~\text{cm}^3~\text{cm}^{-3}$ were used.

Differential effective medium (DEM) theory was introduced by Sen et al. (1981) and Bussian (1983) to model high-frequency dielectric permittivity and DC-electrical conductivity of rocks, respectively (Cosenza et al, 2009). Revil (2000) and later studies (Cosenza et al., 2003; Jougnot and Revil, 2010) then adopted DEM theory to estimate thermal conductivity values of various porous media. The DEM theory had two parameters: λ_s and cementation exponent (*m*). The exponent *m* was first defined by Archie's law and typically ranges from 1.2 to 4.0 for porous media (Friedman, 2005). Both GMM and DEM theory require λ_s as inputs, which, however, is difficult to be determined thus not known for most soils. Thus, in this study, GMM and DEM theory are combined to develop a new relationship between λ_{sat} and ϕ (assuming a constant value of thermal conductivity of water (λ_w)). The best fitted m values for three textural groups (depending on sand content) were determined for 43 soils. The performance of the GMM-DEM approach to estimate λ_{sat} was then tested on another 46 soils and compared with GMM estimates of λ_{sat} using known quartz content or sand content.

2. Model development

2.1. Geometric mean model

The classical geometric mean model (GMM) was first proposed by Lichtenecker (1924). Woodside and Messmer (1961) applied the GMM to calculate the effectivity thermal conductivity of two-phases porous medium, i.e., a solid phase and a saturating fluid phase (e.g., air, water and oil), randomly distributed in the pore space with respect to the direction of heat flow,

$$\lambda = \lambda_s^{1-\phi} \lambda_f^{\phi} \tag{3}$$

where λ_f is the thermal conductivity of the fluid phase. Woodside and Messmer (1961) showed that Eq. (3) gives reliable estimates for unconsolidated sands when the ratio of λ_s to λ_f is less than 20. For most soil minerals, λ_s ranges from 1.8 to 8.8 W m⁻¹ K⁻¹ (Horai, 1971), and thermal conductivity of water (λ_w) is 0.598 W m⁻¹ K⁻¹ at 20 °C. Thus, Eq. (3) can be used to calculate the thermal conductivity of water-saturated soils,

$$\lambda_{\text{sat}} = \lambda_s^{1-\phi} \lambda_w^{\phi} \tag{4}$$

This equation has been extensively used in empirical thermal conductivity models (Donazzi et al., 1979; Ewen and Thomas, 1987; Côté and Konrad, 2005; Lu et al., 2007; Chen, 2008; He et al., 2017). As stated earlier, it is difficult to directly measure λ_s . When the complete mineral composition is known, λ_s can be indirectly estimated using the GMM:

$$\lambda_{\rm s} = \prod_{\rm i} \lambda_{\rm j}^{f_{\rm i}} \quad with \quad \sum_{\rm i} f_{\rm j} = 1 \tag{5}$$

where λ_j (W m⁻¹ K⁻¹) and f_j are the thermal conductivity and volume fraction of the j_{th} forming mineral, respectively. Because the thermal conductivity of quartz (λ_q) is considerably larger than most other soil minerals (λ_o), Johansen (1975) simplified Eq. (5) to include quartz and other minerals only. Then Eq. (5) becomes,

$$\lambda_{\rm s} = \lambda_{\rm q}^{f_{\rm q}} \lambda_{\rm o}^{1-f_{\rm q}} \tag{6}$$

where λ_q is 7.7 W m $^{-1}$ K $^{-1}$; and λ_o is 2.0 W m $^{-1}$ K $^{-1}$ for soils with quartz content (f_q) > 0.2, and 3.0 W m $^{-1}$ K $^{-1}$ for soils with $f_q \leq$ 0.2, respectively.

Combining Eqs. (4) and (6) leads to

$$\lambda_{\text{sat}} = \left(\lambda_{\text{q}}^{f_{\text{q}}} \lambda_o^{1-f_{\text{q}}}\right)^{1-\phi} \lambda_{\text{w}}^{\phi} \tag{7}$$

With Eq. (7), one can estimate λ_{sat} from quartz content and porosity. However, quartz content is usually measured with a combination of X-ray diffraction/X-ray fluorescence techniques, which is expensive and rarely used (Schönenberger et al., 2012). Consequently, quartz content is not commonly known for most soils and is often assumed to be equal either to sand content (f_{sand}) ((Peters-Lidard et al., 1998; Lu et al., 2007; Fu et al., 2021b) or to 50 % of the sand content (Hu et al., 2017; Zhao et al., 2018; He et al., 2021). For Eq. (7), the use of the assumption that $f_q = f_{sand}$ leads to overestimations of λ_{sat} especially for sands (Lu et al., 2007), and using $f_q = 0.5f_{sand}$ significantly underestimates λ_{sat} (He et al., 2020a). Tarnawski et al. (2012) found that for 40 Canadian soils, there was only a weak correlation ($R^2 = 0.33$) between f_q and f_{sand} . Similarly, Calvet et al. (2016) also reported a linear correlation between f_q and f_{sand} with R^2 of 0.67 based on 14 soils in southern France.

2.2. Differential effective medium (DEM) theory

Saturated soil can be regarded as a two-phase mixture of solid and water. Its thermal conductivity can be described by the Maxwell-Garnett equation which was first used for dielectric permittivity (Maxwell, 1873):

$$\frac{\lambda_{\text{sat}} - \lambda_{\text{w}}}{\lambda_{\text{sat}} + 2\lambda_{\text{w}}} = (1 - \phi) \frac{\lambda_{\text{s}} - \lambda_{\text{w}}}{\lambda_{\text{s}} + 2\lambda_{\text{w}}}$$
(8)

where a small volume fraction of 1- ϕ of spherical inclusions (i.e., solid) with a thermal conductivity of λ_s are embedded as isolated spheres in a background or host (i.e., water) with thermal conductivity of λ_w , and λ_{sat} is the effective thermal conductivity of the mixture. The symbols for thermal conductivity in Eq. (8) can also be replaced by dielectric permittivity or electrical conductivity. However, Eq. (8) is only valid for dilute suspensions of spherical solids, which assumes that "the solid spherical inclusions 'see' only the permittivity/electrical conductivity of the background around themselves" (Robinson and Friedman, 2005). Thus, Eq. (8) cannot compute the thermal conductivity of water-saturated soils accurately, because the soil solids are in close contact with each other, and most of the solid particles are non-spherical.

Differential effective medium (DEM) theory is a more realistic way to integrate the thermal interaction between solids and water than the dilute approximation in Eq. (8). The iterative process of the DEM theory can be explained briefly as follows (Fig. 1): at Step 0, the initial homogeneous medium filled with water has a thermal conductivity of $\lambda_{\rm w}$ and a volume of $V_{\rm w}$; at Step k (integer), an infinitesimal increment (d $V_{\rm s}$) of the inclusion phases (e.g., spherical solids) of any size is added into the host phase (i.e., water), then the mixture has an effective thermal conductivity of $\lambda_{\rm k}$ and constitutes the initial medium of the next step (i.e., Step k+1); sequential iterative inclusion of solids into water continues such that at Step n, the desired porosity ($\phi=V_{\rm w}/(V_{\rm w}+V_{\rm s})$) and thermal conductivity ($\lambda_{\rm n}=\lambda_{\rm sat}$) are reached. Here we use DEM theory to estimate thermal conductivity of water-saturated soils with the following equation:

$$\left(\frac{\lambda_{\text{sat}}^i - \lambda_{\text{s}}}{\lambda_w - \lambda_{\text{s}}}\right) \left(\frac{\lambda_w}{\lambda_{\text{est}}^i}\right)^{D^i} = \phi \tag{9}$$

where D^i and λi sat are the depolarization factor and the saturated thermal conductivity in the i_{th} direction with respect to the heat flow direction. Eq. (9) was developed based on a self-similar assumption,

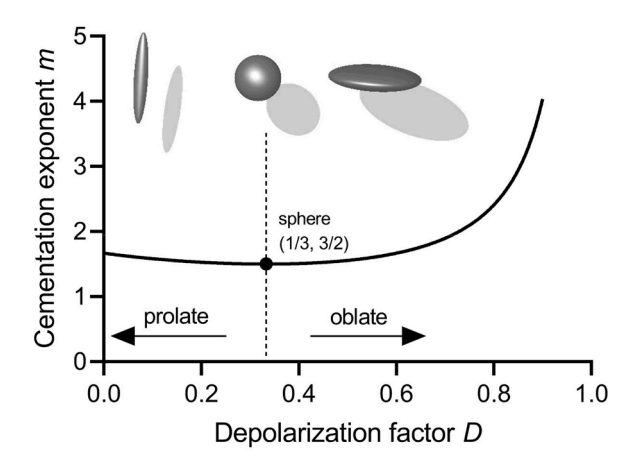


Fig. 2. The effective cementation exponent m as a function of the depolarization factor D for an isotropic medium (Eq. (12)).

which Robinson and Friedman (2001) stated should be applied to a fractal medium of infinitely wide particle size distribution. Theoretically, D^i describes the extent to which the inclusion polarization is reduced according to its shape and orientation with respect to the applied temperature gradient (Lesmes and Friedman, 2005). For a special case of spheroids, D^i can be empirically computed as (Jones and Friedman, 2000):

$$D^{a} = \frac{1}{1 + 1.6(a/b) + 0.4(a/b)^{2}}$$
 (10a)

$$D^b = D^c = 0.5(1 - D^a) \tag{10b}$$

where a, b and c represent the semi-major axial dimension and two semi-minor axial dimensions (b=c), respectively. Specifically, $D^a=D^b=D^c=1/3$ for spherical solids for which Eqs. (8) and (9) form lower and upper bounds for the estimation of λ_{sat} of water-saturated soils (Robinson and Friedman, 2001).

An isotropic version of Eq. (9) can be obtained by averaging the depolarization factors over all possible particle orientations (Mendelson and Cohen, 1982):

$$\lambda_{\text{sat}} = \lambda_{\text{w}} \phi^m \left(\frac{1 - \lambda_{\text{s}} / \lambda_{\text{w}}}{1 - \lambda_{\text{s}} / \lambda_{\text{est}}} \right)^m \tag{11}$$

where m is the effective cementation exponent depending on the particle shape, with an arithmetic correction by Sen (1984) for randomly oriented spheroids:

$$m = \left\langle \frac{(5 - 3D)}{3(1 - D^2)} \right\rangle \tag{12}$$

where D is the depolarization factor along the principal axis of a spheroidal grain and <> denotes an average over the distribution in D at all possible particle orientations. For $i_{\rm th}$ direction, the cementation exponent $m_{\rm i}$ and depolarization factor D^i can be related as $m_{\rm i}=1/(1-D^i)$. The effective cementation exponent m values as a function of D from Eq. (12) are shown in Fig. 2. D=0 represents long, needle-like solids with random orientations (e.g., clay tactoids), with a cementation exponent m of 5/3, which is the upper limit of m for prolate particles; for spherical solids, D=1/3 thus m=3/2 which is the lowest value of m; whereas for oblate, disk-like particles, D approaches 1 and m becomes infinity (Lesmes and Friedman, 2005; Friedman, 2005). More details about the relationship between m and D can be found in Mendelson and Cohen (1982) and Sen (1984).

If we replace all λ terms in Eq. (11) with electrical conductivity terms, Eq. (11) becomes the Bruggeman-Hanai-Sen equation,

$$\sigma_{\text{sat}} = \sigma_{\text{w}} \phi^{m} \left(\frac{1 - \sigma_{\text{s}} / \sigma_{\text{w}}}{1 - \sigma_{\text{s}} / \sigma_{\text{sat}}} \right)^{m} \tag{13}$$

where σ_{sat} , σ_{s} and σ_{w} are electrical conductivities of water-saturated soils, solid particles and water, respectively. At its high-salinity limit $(\sigma_{w} \rightarrow \infty)$, Eq. (13) reduces to Archie's law (Archie, 1942)

$$\lim_{\sigma_{\rm w} \to \infty} \sigma_{\rm sat} = \sigma_{\rm w} \phi^{m} \tag{14}$$

Thus, Revil (2000) stated that m in Eq. (11) is rigorously identical to the cementation exponent in Archie's law and can be obtained from electrical conductivity measurements. For electrical conduction in sand with negligible surface conduction (i.e., $\sigma_s = 0$), the Bruggeman-Hanai-Sen equation (Eq. (13)) reduces to Archie's law (Eq. (14)) at the high-salinity limit. However, for heat transfer in soils, because λ_s (1.8 to 8.8 W m⁻¹ K⁻¹) >> λ_w (~0.6 W m⁻¹ K⁻¹), heat conduction through the soil solids is the dominant pathway. Therefore, we should not expect that m in Eq. (11) is identical to the cementation exponent in Archie's law. In this study, we refer to m as the cementation exponent based on the analog for electrical conductivity, but we did not estimate it from electrical conductivity measurements nor consider any cementation process.

2.3. Derivation of GMM from DEM theory

Although lacking a physical basis, the GMM (Eq. (4)) usually gives reliable $\lambda_{\rm sat}$ estimates of water-saturated soils and rocks (Woodside and Messmer, 1961; Sass et al., 1971; Johansen, 1975; Wang et al., 2020). There have been some attempts to derive a physical basis of the GMM. Zakri et al. (1998) provided a physical basis of GMM from the symmetric Bruggeman equation for ellipsoidal inclusions where their main axes are parallel to the external field, and the 'equivalent depolarization coefficient' follows a special case of a uniform distribution. Simpkin (2010) showed that the GMM can be derived by applying Maxwell's equation (Eq. (8)) and the principle of charge conservation to a mixture in which the components are randomly distributed. However, a more robust theoretical basis for the GMM derived from DEM theory, also known as the asymmetric Bruggeman equation, has never been provided. In this section, starting with DEM theory (Eq. (11)), we present a derivation of the GMM (Eq. (4)).

Eq. (11) can be rewritten as

$$\left(\frac{\lambda_{\text{sat}} - \lambda_{\text{s}}}{\lambda_{\text{w}} - \lambda_{\text{s}}}\right) \left(\frac{\lambda_{\text{w}}}{\lambda_{\text{sat}}}\right)^{1 - 1/m} = \phi$$
(15)

Taking the logarithm of both sides of Eq. (15) gives

$$\ln\left(\frac{\lambda_{\text{sat}}^{1-1/m}}{\lambda_{\text{s}} - \lambda_{\text{sat}}}\right) - \ln\left(\frac{\lambda_{\text{w}}^{1-1/m}}{\lambda_{\text{s}} - \lambda_{\text{w}}}\right) = \ln\frac{1}{1 - (1 - \phi)} - \ln\frac{1}{1 - 0}$$
(16)

Eq. (16) can be rewritten in an integral form as

$$\int_{\lambda_{w}}^{\lambda_{\text{sat}}} \left(\frac{\lambda + (1 - 1/m)(\lambda_{s} - \lambda)}{(\lambda_{s} - \lambda)\lambda} \right) d\lambda = \int_{0}^{1 - \phi} \frac{d\phi_{s}}{1 - \phi_{s}}$$
(17)

Eq. (17) represents the iteration process such that after n steps, a total volume fraction of 1- φ of solid inclusions is added into the water phase and the corresponding λ changes from λ_w representing a homogenous water phase to $\lambda_{\rm sat}$ representing a water-saturated soil. For an infinitesimal increment of soil solids, $d\varphi_s$, at Step k+1 (Fig. 1), Eq. (17) yields,

$$\frac{\lambda_k + (1 - 1/m)(\lambda_s - \lambda_k)}{(\lambda_s - \lambda_k)\lambda_k}(\lambda_{k+1} - \lambda_k) \cong \frac{\mathrm{d}\phi_s}{1 - k \times \mathrm{d}\phi_s}$$
(18)

Eq. (18) can be rearranged to give the thermal conductivity ratio $\frac{\lambda_{k+1}}{\lambda_k}$

Table 1 Soil name, texture, particle size distribution, porosity (ϕ) and sources of soils in the calibration dataset.

Soil ID	Soil name	Texture	Particle si	ze distribution		ф	Sources	
			Sand	Silt	Clay	${\rm cm}^3~{\rm cm}^{-3}$		
1	Accusand 12/20	sand	1.00	0.00	0.00	0.317	Deepagoda et al. (2016)	
2	Accusand 20/30	sand	1.00	0.00	0.00	0.332	Deepagoda et al. (2016)	
3	Accusand 30/40	sand	1.00	0.00	0.00	0.336	Deepagoda et al. (2016)	
4	Accusand 40/50	sand	1.00	0.00	0.00	0.347	Deepagoda et al. (2016)	
5	Accusand 50/70	sand	1.00	0.00	0.00	0.336	Deepagoda et al. (2016)	
6	-	sand	0.94	0.01	0.05	0.40	Lu et al. (2007)	
7	-	sand	0.93	0.01	0.06	0.40	Lu et al. (2007)	
8	-	sandy loam	0.67	0.21	0.12	0.48	Lu et al. (2007)	
9	-	loam	0.40	0.49	0.11	0.58, 0.51, 0.47	Lu et al. (2007)	
10	-	silt loam	0.27	0.51	0.22	0.50	Lu et al. (2007)	
11	-	silt loam	0.11	0.70	0.19	0.51	Lu et al. (2007)	
12	-	silty clay loam	0.19	0.54	0.27	0.55, 0.51, 0.47	Lu et al. (2007)	
13	-	silty clay loam	0.08	0.60	0.32	0.51	Lu et al. (2007)	
14	-	clay loam	0.32	0.38	0.30	0.51	Lu et al. (2007)	
15	-	loam	0.50	0.41	0.09	0.48	Lu et al. (2007)	
16	-	sand	0.92	0.07	0.01	0.40	Lu et al. (2007)	
17	_	silty clay	0.07	0.50	0.43	0.52	Lu et al. (2011)	
18	-	sand	0.94	0.01	0.05	0.40	Lu et al.(2013)	
19	_	silt loam	0.02	0.73	0.25	0.55	Lu et al. (2007)	
20	_	sand	0.91	0.03	0.06	0.47, 0.43, 0.40	Fu et al. (2021a)	
21	_	sandy loam	0.52	0.36	0.12	0.53, 0.49, 0.45	Fu et al. (2021a)	
22	_	silt loam	0.34	0.53	0.13	0.57, 0.53, 0.49	Fu et al. (2021a)	
23	_	sand	1.00	0.00	0.00	0.43, 0.40, 0.37	Fu et al. (2021a)	
24	_	silt loam	0.21	0.67	0.12	0.60, 0.57, 0.53	Fu et al. (2021a)	
25	_	clay loam	0.24	0.49	0.27	0.60, 0.58, 0.55	Fu et al. (2021a)	
26	Pale brown	silt loam	0.25	0.58	0.17	0.44	Hailemariam et al. (2017)	
27	Brown	silt loam	0.27	0.53	0.20	0.46	Hailemariam et al. (2017)	
28	Pale black	silt loam	0.10	0.65	0.25	0.48	Hailemariam et al. (2017)	
29	Ottawa sand	sand	1.00	0.00	0.00	0.37	Nikolaev et al. (2013)	
30	Richmond Hill	loam	0.52	0.32	0.15	0.57	Nikolaev et al. (2013)	
31	A	sand	1.00	1.00	1.00	0.49, 0.46, 0.42, 0.34	Chen (2008)	
32	В	sand	1.00	1.00	1.00	0.55, 0.51, 0.47, 0.43	Chen (2008)	
33	C	sand	1.00	1.00	1.00	0.55, 0.51, 0.47, 0.43	Chen (2008)	
34	D	sand	1.00	1.00	1.00	0.47, 0.43, 0.40, 0.35	Chen (2008)	
35	L-soil	sand	0.89	0.06	0.05	0.47, 0.43, 0.40, 0.33	Campbell et al. (1994)	
35 36	L-S011 Mokins	sand silt loam	0.89	0.06	0.05	0.43	Campbell et al. (1994)	
					0.25			
37	Palouse-A	silt loam	0.11	0.68	0.21	0.52	Campbell et al. (1994)	
38	Palouse-B	silty clay	0.09	0.44		0.57	Campbell et al. (1994)	
39	Royal	sandy loam	0.54	0.32	0.15	0.49	Campbell et al. (1994)	
40	Salkum	silt loam	0.19	0.59	0.23	0.59	Campbell et al. (1994)	
41	Walla Walla	silt loam	0.23	0.63	0.14	0.53	Campbell et al. (1994)	
42	Volkmar	sandy loam	0.72	0.16	0.12	0.46	Campbell et al. (1994)	
43	Norfolk	sandy loam	0.75	0.10	0.15	0.41	Hopmans and Dane (1986	

$$\frac{\lambda_{k+1}}{\lambda_k} = 1 + \frac{\mathrm{d}\phi_s}{1 - k \times \mathrm{d}\phi_s} \frac{\left(\frac{\lambda_s}{\lambda_k} - 1\right)}{1 + (1 - 1/m)\left(\frac{\lambda_s}{\lambda_k} - 1\right)} \tag{19}$$

We considered a special case that k = 0 (i.e., $\lambda_k = \lambda_w$) first,

$$\frac{\lambda_1}{\lambda_0} = \frac{\lambda_1}{\lambda_w} = 1 + d\phi_s \frac{\left(\frac{\lambda_s}{\lambda_w} - 1\right)}{1 + (1 - 1/m)\left(\frac{\lambda_s}{\lambda_w} - 1\right)} > \left(\frac{\lambda_s}{\lambda_w}\right)^{d\phi_s}$$
(20)

The inequality in Eq. (20) holds when m satisfies that,

$$m > \frac{1}{1 - \left\lceil \frac{\left(\frac{\lambda_{n}}{\lambda_{w}} - 1\right)}{\ln\left(\frac{\lambda_{n}}{\lambda_{w}}\right)} - 1\right\rceil / \left(\frac{\lambda_{n}}{\lambda_{w}} - 1\right)}$$

$$(21)$$

A detailed derivation of Eq. (21) is provided in Appendix A. As k increases, λ_k increases and thus $\frac{\lambda_{k+1}}{\lambda_k}$ in Eq. (19) decreases. When k approaches n-1,

$$\lim_{k \to n-1} \frac{\lambda_{k+1}}{\lambda_k} = 1 < \left(\frac{\lambda_s}{\lambda_w}\right)^{d\phi_s} \tag{22}$$

Thus, we specified a value of m

$$\left(m > \frac{1}{1 - \left[\frac{\left(\frac{\lambda_{g}}{\lambda_{g_{w}}} \cdot 1\right)}{\ln\left(\frac{\lambda_{g}}{\lambda_{g_{w}}}\right) - 1\right] / \left(\frac{\lambda_{g}}{\lambda_{w}} - 1\right)}\right) \text{ satisfying,}$$

$$\frac{\lambda_{\text{sat}}}{\lambda_{\text{w}}} = \frac{\lambda_{\text{sat}}}{\lambda_{n-1}} \frac{\lambda_{n-1}}{\lambda_{n-2}} \cdots \frac{\lambda_{k+1}}{\lambda_{k}} \cdots \frac{\lambda_{1}}{\lambda_{\text{w}}}$$

$$= \prod_{k=0}^{k=n-1} \left[1 + \frac{\mathrm{d}\phi_s}{1 - k \times \mathrm{d}\phi_s} \frac{\left(\frac{\lambda_s}{\lambda_k} - 1\right)}{1 + (1 - 1/m)\left(\frac{\lambda_s}{\lambda_k} - 1\right)} \right] = \left(\frac{\lambda_s}{\lambda_w}\right)^{n \times \mathrm{d}\phi_s} \tag{23}$$

where $n \times d\phi_s$ represents the total volume fraction of inclusion phases $(1-\phi)$ during the iteration process, thus $1-n \times d\phi_s$ is exactly ϕ . Then Eq. (22) becomes the GMM between λ_{sat} , λ_w and λ_s as represented by Eq. (4).

In summary, the derivations above provide a firm justification for the GMM from DEM theory, which means that the GMM and DEM become identical with appropriate m values. If we rewrite the GMM (Eq. (4)) as,

Table 2 Soil name, texture, particle size distribution, quartz content, particle density (ρ_s) , porosity (ϕ) and sources of soils in the validation dataset.

Soil ID	Soil name	Texture	Particle size distribution		Quartz content	ρ_{s}	ф	Sources	
			Sand	Silt	Clay		${\rm g~cm^{-3}}$	${\rm cm}^3~{\rm cm}^{-3}$	
44	Acadia	silt loam	0.33	0.57	0.10	0.51	2.71	0.55	Tarnawski et al. (2015)
45	Cumberland	sandy loam	0.61	0.34	0.05	0.61	2.71	0.45	Tarnawski et al. (2015)
46	Pugwash	sandy loam	0.57	0.37	0.05	0.63	2.68	0.40	Tarnawski et al. (2015)
47	Stable Island	sand	1.00	0.00	0.00	1.00	2.66	0.36	Tarnawski et al. (2015)
48	Cornwallis-Annapolis-V	loamy sand	0.85	0.12	0.03	0.72	2.66	0.4	Tarnawski et al. (2015)
49	Pugwash-Annapolis Valley	sandy loam	0.56	0.38	0.06	0.65	2.68	0.51	Tarnawski et al. (2015)
50	Queens-Annapolis Valley	silt loam	0.22	0.66	0.12	0.34	2.78	0.57	Tarnawski et al. (2015)
51	Orthic Podzol-1	loam	0.50	0.42	0.08	0.66	2.64	0.44	Tarnawski et al. (2015)
52	Orthic Podzol-2	loam	0.51	0.40	0.09	0.58	2.66	0.42	Tarnawski et al. (2015)
53	Orthic Podzol-3	loamy sand	0.83	0.14	0.03	0.54	2.66	0.41	Tarnawski et al. (2015)
54	Caribou	silt loam	0.03	0.82	0.15	0.57	2.59	0.54	Tarnawski et al. (2015)
55	Victoria	silt loam	0.00	0.83	0.17	0.56	2.54	0.45	Tarnawski et al. (2015)
56	Juniper	silt loam	0.24	0.66	0.1	0.55	2.57	0.62	Tarnawski et al. (2015)
57	Queens	silt loam	0.26	0.64	0.1	0.60	2.59	0.54	Tarnawski et al. (2015)
58	Fundy	silty clay loam	0.00	0.67	0.33	0.39	2.71	0.54	Tarnawski et al. (2015)
59	Beach	sand	0.93	0.05	0.02	0.35	2.73	0.43	Tarnawski et al. (2015)
60	Field 9	loamy sand	0.79	0.17	0.03	0.42	2.69	0.48	Tarnawski et al. (2015)
61	Brainsville	silt loam	0.36	0.56	0.08	0.28	2.70	0.43	Tarnawski et al. (2015)
62	North Gower	silt loam	0.07	0.75	0.18	0.17	2.76	0.51	Tarnawski et al. (2015)
63	Matilda	loamy sand	0.71	0.25	0.04	0.41	2.71	0.46	Tarnawski et al. (2015)
64	Uplands	sand	0.89	0.10	0.01	0.38	2.76	0.39	Tarnawski et al. (2015)
65	Lyons	sandy loam	0.56	0.37	0.07	0.36	2.75	0.38	Tarnawski et al. (2015)
66	Uplands	loamy sand	0.84	0.14	0.02	0.38	2.74	0.44	Tarnawski et al. (2015)
67	North Gower	silt loam	0.32	0.54	0.14	0.25	2.76	0.45	Tarnawski et al. (2015)
68	Byerson series	silt loam	0.17	0.69	0.14	0.38	2.69	0.55	Tarnawski et al. (2015)
69	Inwood series	silt loam	0.22	0.55	0.23	0.20	2.79	0.41	Tarnawski et al. (2015)
70	Osborne series	silt loam	0.03	0.76	0.21	0.21	2.74	0.63	Tarnawski et al. (2015)
71	Almassippi series	loamy sand	0.81	0.16	0.03	0.61	2.71	0.47	Tarnawski et al. (2015)
72	Paddockwood	silt loam	0.00	0.74	0.26	0.48	2.69	0.41	Tarnawski et al. (2015)
73	Gronlid Orthic	sandy loam	0.67	0.27	0.06	0.61	2.70	0.45	Tarnawski et al. (2015)
74	Fox Valley	silt loam	0.02	0.83	0.15	0.37	2.70	0.53	Tarnawski et al. (2015)
75	Asquith Orthic	loamy sand	0.83	0.14	0.03	0.67	2.68	0.42	Tarnawski et al. (2015)
76	Bradwell Orthic	sandy loam	0.68	0.27	0.05	0.63	2.68	0.45	Tarnawski et al. (2015)
77	Lethbridge	silt loam	0.38	0.52	0.1	0.55	2.64	0.55	Tarnawski et al. (2015)
78	FSJ # 1	silty clay	0.00	0.58	0.42	0.21	2.74	0.51	Tarnawski et al. (2015)
79	FSJ # 2	silty clay	0.00	0.58	0.42	0.19	2.72	0.50	Tarnawski et al. (2015)
80	Vanderhoof	silty clay loam	0.00	0.70	0.30	0.27	2.71	0.51	Tarnawski et al. (2015)
81	PG # 1	silty clay	0.00	0.59	0.41	0.17	2.78	0.52	Tarnawski et al. (2015)
82	PG # 2	silty clay loam	0.00	0.67	0.33	0.17	2.77	0.53	Tarnawski et al. (2015)
83	9718 SW	silt loam	0.32	0.58	0.1	0.37	2.76	0.52	Tarnawski et al. (2015)
84	Ottawa sand C-109	sand	1.00	0.00	0.00	1.00	2.65	0.32, 0.40	Tarnawski et al. (2013)
85	Ottawa sand C-190	sand	1.00	0.00	0.00	1.00	2.65	0.32, 0.40	Tarnawski et al. (2013)
86	Toyoura	sand	1.00	0.00	0.00	0.87	2.65	0.38, 0.40	Tarnawski et al. (2013)
87	Toyoura	sand	1.00	0.00	0.00	0.87	2.65	0.40	Kasubuchi et al. (2007)
88	Red Yellow	silty clay loam	0.34	0.23	0.43	0.58	2.70	0.60	Kasubuchi et al. (2007)
89	Kuroboku	loam	0.28	0.58	0.14	0.45	2.44	0.65	Kasubuchi et al. (2007)

$$\lambda_{s} = \left(\frac{\lambda_{sat}}{\lambda_{w}^{\phi}}\right)^{\frac{1}{1-\phi}} \tag{24}$$

Then by inserting Eq. (24) into Eq. (11), we obtained the following expression:

$$\lambda_{\text{sat}} = \lambda_{\text{w}} \phi^{m} \left(\frac{1 - \left(\frac{\lambda_{\text{sat}}}{\lambda_{\text{w}}} \right)^{\frac{1}{1 - \phi}}}{1 - \left(\frac{\lambda_{\text{sat}}}{\lambda_{\text{w}}} \right)^{\frac{\phi}{1 - \phi}}} \right)^{m}$$
(25)

Eq. (25), denoted hereafter as "DEM-GMM", is developed based on a combination of differential effective medium theory and the geometric mean method. Once m is known, one can estimate $\lambda_{\rm sat}$ from φ with Eq. (25), where $\lambda_{\rm w}$ is assumed to have a constant value (i.e., 0.598 W m⁻¹ K⁻¹) at room temperature (influence of temperature on Eq. (25) will be investigated in Section 4.2). Several facts regarding Eq. (25) need be stated here. First, as stated earlier, m is not identical to the cementation exponent defined by Archie's law, thus it is not expected to be accurately estimated from electrical conductivity measurements. Second, the effects of grain contact are assumed to be zero (i.e., dilute assumption at

each iteration step) during the iteration process in the DEM theory. However, continuous solid phase or the solid-to-solid contact through a thin water film (i.e., water bridge) in saturated soils cannot be neglected, thus fitting m also accounts for the errors from this assumption. Third, except for the special case of m=2, numerical methods must be used to solve Eq. (25) for $\lambda_{\rm sat}$ implicitly (e.g., Glover et al., 2010; Niu et al., 2016; Revil 2000). In this study, we used the Solver in Excel to solve Eq. (25) implicitly. Besides, the DEM-GMM approach has been implemented into the Python programming language: the source code as well as additional documentation are also provided in the Acknowledgements.

3. Datasets

In this study, data representing 89 soils were collated from the literature and used to develop and validate the DEM-GMM approach. Constraints were imposed on the dataset such that all of the soils had λ_{sat} values measured with standard techniques at room temperature (i.e., $20{-}25~^\circ\text{C}$), particle size distribution, and porosity. These soils were then divided into a calibration dataset of 43 soils and a validation dataset of 46 soils, spanning a range of soil textures and porosities. The 46 soils in the validation dataset also had available quartz content to evaluate the

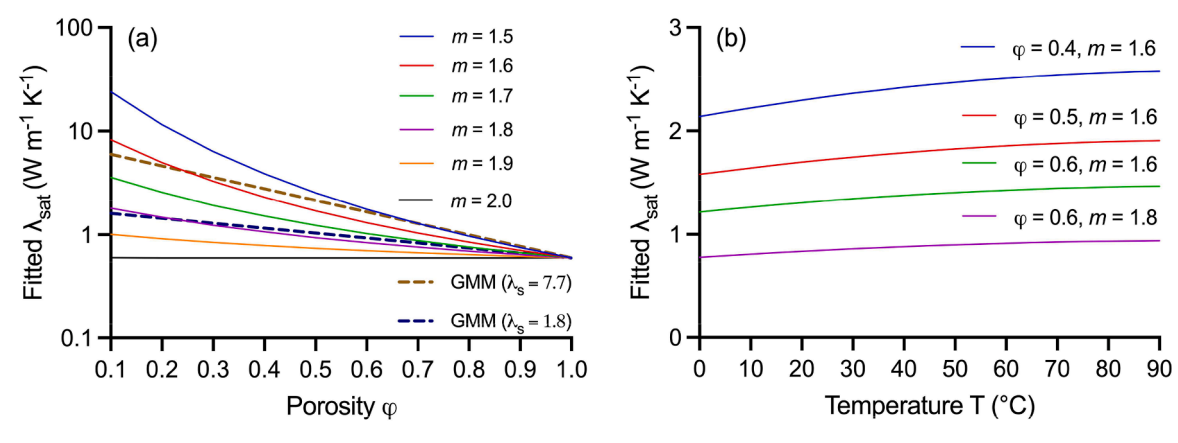


Fig. 3. Saturated thermal conductivity λ_{sat} values determined by the DEM-GMM approach (Eq. (25)) as a function of (a) porosity (φ) for various m values and $\lambda_{w} = 0.598$ W m⁻¹ K⁻¹; (b) the effect of temperature (T) on λ_{sat} for various groups of φ and T. The two dash curves in Fig. 3a represent the λ_{sat} values determined by the GMM using two representative λ_{s} values.

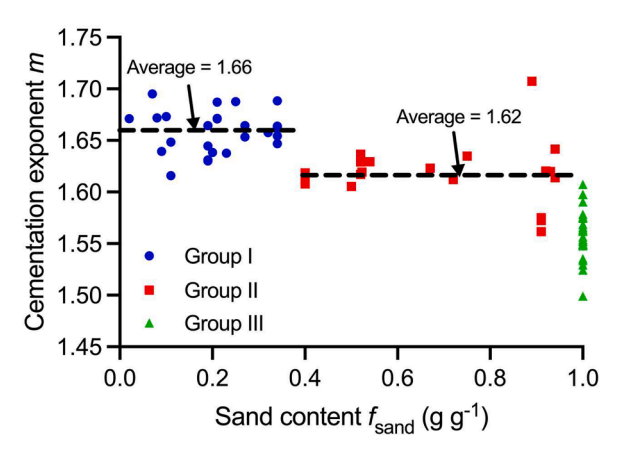


Fig. 4. The cementation exponent (m) as a function of sand content ($f_{\rm sand}$) determined via the DEM-GMM approach for Soils 1–43 in the calibration dataset.

Table 3 Number of soils and fitted m values for three textural groups (i.e., Group I ($f_{\text{sand}} < 0.4$), Group II ($0.4 \le f_{\text{sand}} < 1$) and Group III ($f_{\text{sand}} = 1$)) in the calibration and validation datasets.

	Calibrati	on dataset		Validation dataset			
	Group I	Group II	Group III	Group I	Group II	Group III	
Number of soils	18	14	11	24	17	5	
m	1.659	1.618	$-0.34\phi + 1.70$	-	-	-	

performance of the DEM-GMM approach by comparing results to the GMM (Eq. [7]) estimates using quartz contents as inputs. Tables 1 and 2 present the basic soil physical properties and the sources of the 89 soils.

4. Results and discussion

4.1. Factors affecting the DEM-GMM estimated λ_{sat} values

The DEM-GMM (Eq. [25]) λ_{sat} estimates depend on λ_w , ϕ and m. The thermal conductivity of water λ_w depends on temperature and is approximately 0.6 W m⁻¹ K⁻¹ at room temperature (temperature effect will be discussed later). Porosity ranges from 35 % to 50 % for most coarse-textured soils and from 40 % to 60 % for most fine-textured soils (Hao et al., 2008). If the ϕ value is known, m is the only unknown

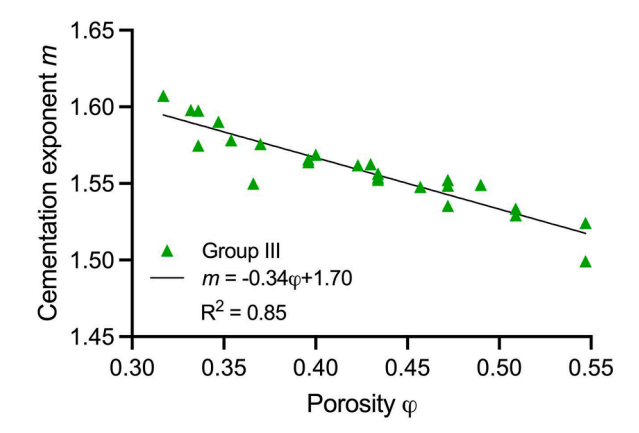


Fig. 5. The cementation exponent (m) as a function of porosity (ϕ) for soils in Group III $(f_{sand} = 1)$ of the calibration dataset.

parameter. Fig. 3a illustrates the influence of m on DEM-GMM λ_{sat} estimates (Eq. (25)) as a function of ϕ . In general, for all m values, λ_{sat} decreases as ϕ increases. As ϕ increases, the number of contacts between soil solids and the fraction of soil solids in the bulk soil decrease, thus, the magnitude of λ_{sat} decreases. At $\phi=1$, $\lambda_{sat}=\lambda_{w}$ for all m values. Porosity equal to unity means that there are no soil solids present, thus the λ_{sat} value is indeed λ_w . It is obvious that as m increases, both the magnitude of λ_{sat} and the rate of decrease in λ_{sat} with respect to φ decrease. For small m values, the DEM-GMM approach gives unreasonably large λ_{sat} values at low ϕ . For example, when $\phi = 0.1$ and m = 1.5, the DEM-GMM λ_{sat} estimate is 23.9 W m⁻¹ K⁻¹, which is twice the value of λ_0 , i.e., the highest among all mineral compositions within soils. This is not a major problem for the DEM-GMM approach when applied to natural soils for which ϕ values generally range from 0.4 to 0.6. At m =2.0, λ_{sat} becomes independent of ϕ and is nearly equal to λ_{w} (i.e., 0.598 W m⁻¹ K⁻¹). In this study, 43 soils in the calibration dataset yielded mvalues ranging from 1.50 to 1.71 and the lower bound is exactly the theoretical lower limit of *m* from Eq. [13] when soil solids are uniformly packed spheres.

In the prior analysis, we assumed the value of λ_w to be constant (i.e., 0.598 W m⁻¹ K⁻¹) at room temperature. However, as temperature (*T*) increases, λ_w also gradually increases, thus affecting λ_{sat} estimates with the DEM-GMM approach. The dependence of λ_w on *T* for 0 °C < T < 90 °C (Ramires et al., 1995) is expressed as,

$$\lambda_{\rm w}^* = -1.48445 + 4.12292 \, T^* - 1.63866 \, T^{*2} \tag{26a}$$

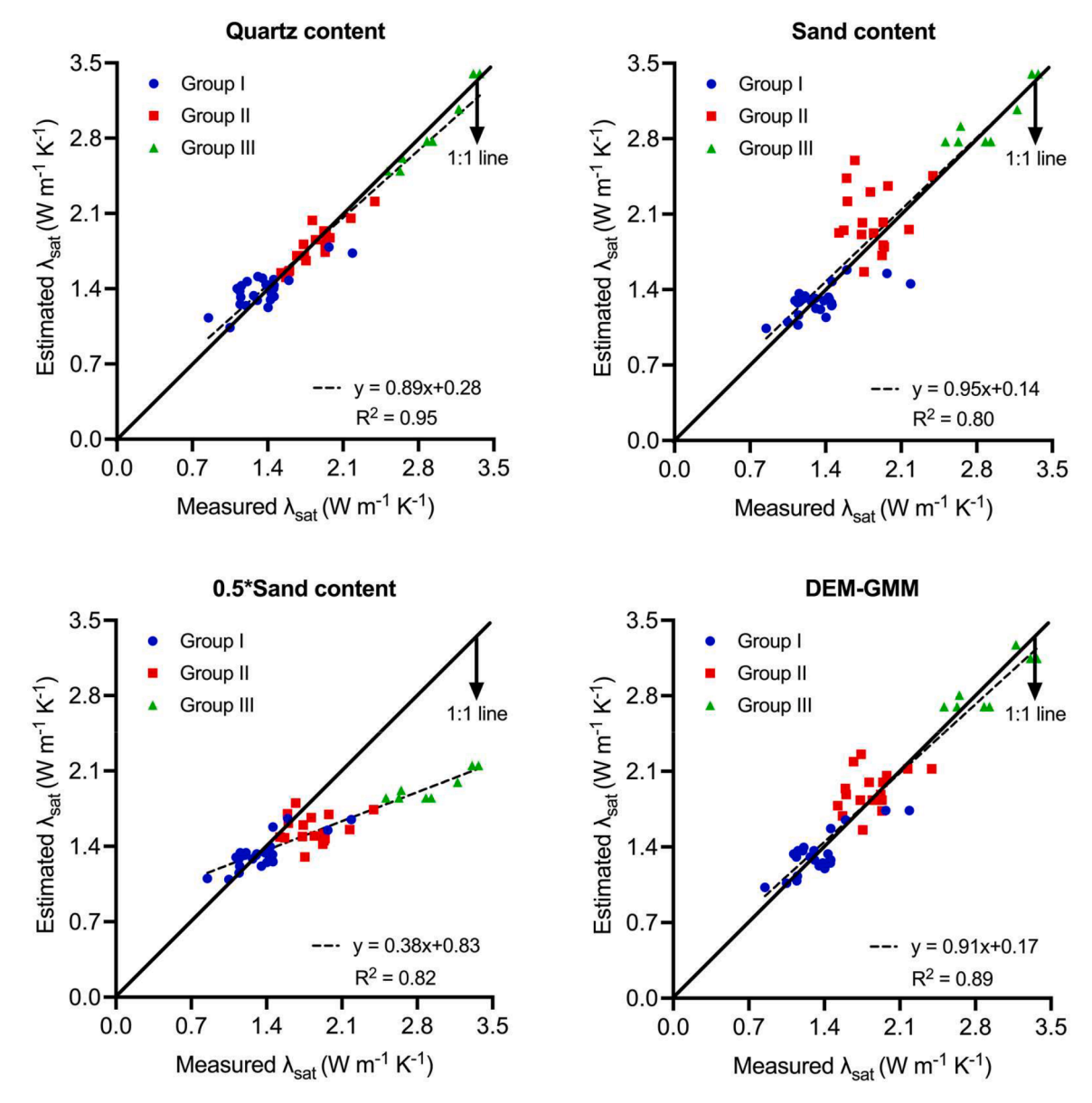


Fig. 6. Comparison of λ_{sat} values estimated with the geometric mean method (Eq. (7)) using inputs of measured quartz content, or setting quartz content equal to sand content, or setting quartz content equal to 0.5 \times sand content, and by the DEM-GMM approach (Eq. (25)) versus measured λ_{sat} for Soil 44-89 in the validation dataset. The solid lines are the 1:1 lines. Groups I, II and III represent soils with $f_{sand} < 0.4$, $0.4 \le f_{sand} < 1$ and $f_{sand} = 1$, respectively.

Table 4 Estimated λ_{sat} values for the validation set of Soils 44–89 calculated with the geometric mean method (Eq. [5]) using inputs of quartz content, quartz content equal to sand content, quartz content equal to 0.5 × sand content, and the DEM-GMM approach (Eq. (22)). Groups I, II and III represent soils with $f_{sand} < 0.4$, $0.4 \le f_{sand} < 1$ and $f_{sand} = 1$, respectively. The superscript numbers represent the order of performance (e.g., 1 indicates the best and 4 indicates the worst).

	Group I		Group II	Group II		Group III		All	
	RMSE	Bias	RMSE	Bias	RMSE	Bias	RMSE	Bias	
Quartz content	0.183	0.032	0.104	-0.037	0.097	-0.053	0.147^{1}	-0.005 ¹	
Sand content	0.217	-0.064	0.415	0.227	0.165	0.053	0.295^{3}	0.056^{3}	
$0.5 \times sand content$	0.186	-0.027	0.362	-0.272	1.001	-0.978	0.476^4	-0.268^4	
DEM-GMM	0.173	-0.029	0.245	0.094	0.172	-0.036	0.202^{2}	0.013^{2}	

$$T^* = \frac{T + 293.15}{298.15} \tag{26b}$$

$$\lambda_{\rm w}^* = \frac{\lambda_{\rm w}}{0.6065} \tag{26c}$$

where T^* and λ_w^* are relative temperature and relative thermal

conductivity of water with respect to those at 298.15 K (25 °C), respectively. From Eq. (26a), $\lambda_{\rm w}$ and T show a quadratic relationship such that as T increases, $\lambda_{\rm w}$ increases, thus also leading to an increase in $\lambda_{\rm sat}$ estimated with the DEM-GMM approach (Eq. (25)). For saturated soils, there is no void space through which vapor can move, thus latent heat transfer is small and conductive heat transfer is the dominant

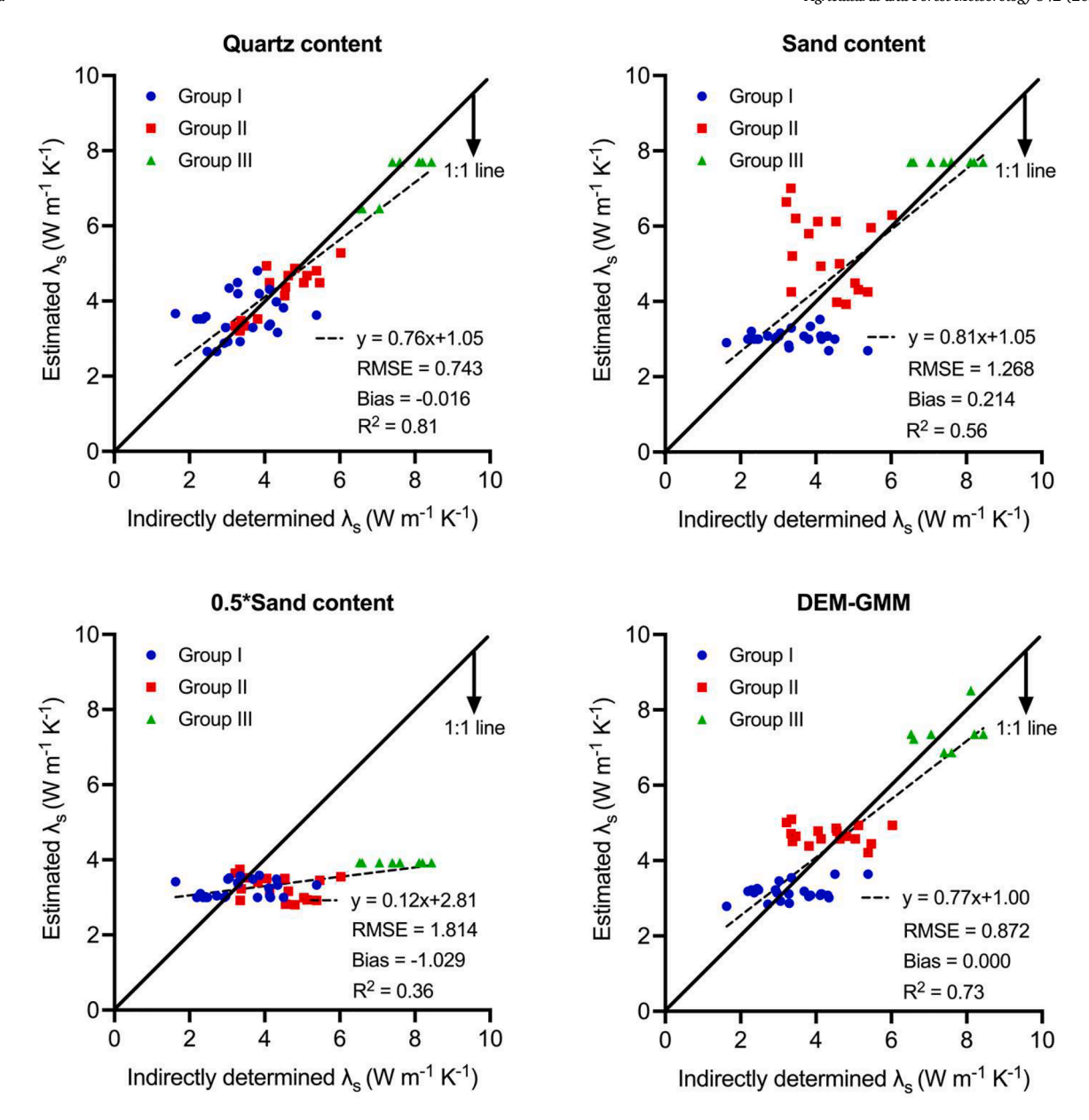


Fig. 7. Comparison of λ_s values estimated with the geometric mean method (Eq. (6)) using inputs of measured quartz content, or by setting quartz content equal to sand content or to $0.5 \times \text{sand}$ content, and by the DEM-GMM approach (Eq. [25]) versus λ_s indirectly estimated from measured λ_{sat} (Eq. (24)) for Soil 44–89 in the validation dataset. The solid lines are the 1:1 lines. Groups I, II and III represent soils with $f_{\text{sand}} < 0.4$, $0.4 \le f_{\text{sand}} < 1$ and $f_{\text{sand}} = 1$, respectively.

mechanism (Smits et al., 2013). In Fig. 3b, we examine $\lambda_{\rm sat}$ versus T from 0 °C to 90 °C and find similar trends for various groups of m and ϕ . With increasing T, $\lambda_{\rm sat}$ gradually increases and finally becomes stable when T approaches 90 °C. For all groups of m and ϕ , $\lambda_{\rm sat}$ increases by 20.6 % from 0 °C to 90 °C, which is also the percentage of increase in $\lambda_{\rm w}$ over this range. This agrees with the results reported by Nikolaev et al. (2013) that $\lambda_{\rm sat}$ of Ottawa sand and Richmond Hill fine sandy loam increased by about 20 % from 2 °C to 92 °C. Note that, at the range of room temperature (20–25 °C), $\lambda_{\rm sat}$ increases by only 0.034, 0.025, 0.019 and 0.012 W m⁻¹ K⁻¹ for ϕ = 0.4 and m = 1.6, ϕ = 0.5 and m = 1.6, ϕ = 0.6 and m = 1.8, respectively. Thus, we hypothesize that temperature effects on $\lambda_{\rm sat}$ at room temperature can be ignored, and we use $\lambda_{\rm w}$ at 20 °C, 0.598 W m⁻¹ K⁻¹, in the following sections.

4.2. Factors affecting m

By fitting Eq. (25) to the measured λ_{sat} (ϕ) values, we obtained parameter m values for the 43 soils in the calibration dataset. We then

analyzed possible correlations between m and particle size distribution and porosity and found that correlations were relatively weak. In Fig. 4, the strongest correlation is plotted as the fitted parameter m ranging from 1.50 to 1.71 versus f_{sand} ranging from 0.02 to 1 g g⁻¹ with R² = 0.64. Generally, the m values decrease as $f_{\rm sand}$ increases and their relation behaves more like a step function or a piecewise-constant function. This is because sand grains are generally more spherical (*m* close to 1.5), while clay particles are flat, disk-like or long, needle-like tactoids, thus having a greater value of m (Mendelson and Cohen, 1982; Friedman, 2005). For example, Soils 1–5 are silica sand with high sphericity (≥ 0.9) which have m values ranging from 1.575 to 1.607, not far from the theoretical lower bound of m for mixtures of spherical grains. Sand content can also be regarded as an indicator of particle size range, which also influences the value of m. Although effective medium theory suggests that m is independent of particle size range (Sen et al., 1981; Mendelson & Cohen, 1982), Niu and Zhang (2018) report that this only holds at $\phi > 0.65$ for granular soil samples. For the 43 soils in our calibration dataset, porosities range from 0.32 to 0.60. Thus, for these

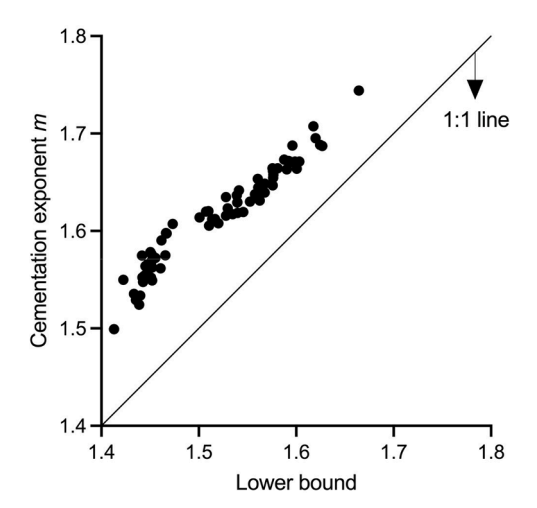


Fig. A.1. Cementation exponent (m) values determined via the DEM-GMM approach for Soils 1-43 in the calibration dataset versus their lower bound values (i.e., right side of Eq. (A.4)).

soil conditions the particle size range is also expected to influence m such that the larger the mean particle size (e.g., sands) the smaller the m values, as shown in Fig. 4.

Based on our observations, we divided the soils into three textural groups depending on their sand contents: Group I ($f_{sand} < 0.4$), Group II (0.4 \leq f_{sand} < 1) and Group III (f_{sand} = 1). We noticed that such a classfication is similar to textural groups based on $\lambda(\theta)$ of unsaturated soils by Fu et al. (2023), in which three groups were: Group I (f_{sand} < 0.4), Group II (Remainder) and Group III (sand). The number of soils included in each group in the calibration and validations steps are presented in Table 3. For Groups I and II, fitted m values are distributed in relatively narrow ranges, 1.62 to 1.70 and 1.56 to 1.71, respectively. The average m values for soils in Group I and II are 1.66 and 1.62, respectively. For the 11 soils in Group III, fitted m values range from 1.50 to 1.61. Because all of the soils in Group III have $f_{\text{sand}} = 1$, we correlated the m with porosity and found a strong linear relationship (m = -1.34 ϕ +1.70) with an R² of 0.85 (Fig. 5). This indicates that m is not only affected by the particle size but also by porosity. This agrees with Niu and Zhang (2018) who report that m decreases as ϕ increases for granular soil samples (Fig. 2 in their study). Glover (2009) reports that the value of the cementation exponent m increases as the degree of connectedness of the pore network diminishes, which is affected by porosity and pore connectivity (see Eq. (18) in Glover, 2009).

4.3. DEM-GMM estimates of λ_{sat}

With the fitted *m* values for each group determined in the previous section, one can estimate λ_{sat} from ϕ with the DEM-GMM approach (Eq. (25)). The DEM-GMM approach does not require estimates of quartz content. In this section, we compare DEM-GMM estimates to the GMM estimates (Eq. (7)) for three quartz input conditions: (i) quartz content (hereafter QC), (ii) the assumption that sand content is equal to the quartz content (hereafter SC), or (iii) $0.5 \times sand$ content is equal to the quartz content (hereafter 0.5SC). Fig. 6 shows the estimated λ_{sat} values versus the measured ones for Soils 44-89 in the validation dataset which are classified into Groups I, II and III as defined earlier. For Group I, the four λ_{sat} estimate approaches perform very similarly such that the measured and estimated results are depicted together for most data points, except for some scattered data points for the SC approach. The RMSEs and bias values range from 0.173 to 0.217 W m^{-1} K⁻¹ and -0.064 to 0.032 W m^{-1} K $^{-1}$, respectively (Table 4). Although earlier studies show that the QC approach gives accurate λ_{sat} estimates (Woodside and Messmer, 1961; Johnsen, 1975; Côté and Konrad, 2005; Wang et al., 2020), we found the QC approach to overestimate λ_{sat} for soils in Group

I, which agreed with the findings of Barry-Macaulay et al. (2015) that the QC estimated and measured values on five fine-textured soils showed a very large scatter and overestimation (Fig. 1b in Barry-Macaulay et al., 2015). Côté and Konrad (2007) also found that for several clay soils, minerals other than quartz play an important role in determining λ_s which undermines simplification of Eq. (5) to Eq. (6).

The performances of the four approaches differ most for Group II: the OC approach performs best with RMSE of 0.104 W m⁻¹ K⁻¹ and a bias of -0.037 W m⁻¹ K⁻¹, which are much better than the other three approaches. The DEM-GMM is second best (RMSE and bias are 0.247 W m⁻¹ K⁻¹ and 0.094 W m⁻¹ K⁻¹, respectively), and it provides more accurate estimates than either SC or 0.5 SC approaches. The SC approach over predicts λ_{sat} with the largest RMSE of 0.415 W $m^{-1}\,K^{-1}$ and a bias of 0.227 W m⁻¹ K⁻¹. This is in accordance with overestimations reported by others using the assumption that quartz content is close to the sand content, especially for coarse-textured soils (Bristow, 2002; Lu et al., 2007). In contrast, the 0.5SC approach significantly underestimates λ_{sat} for soils in Group II with a bias of -0.272 W m⁻¹ K⁻¹. Similar results were also presented in Fig. 2 in He et al. (2020a). All approaches except 0.5SC give reliable λ_{sat} estimates for soils in Group III with RMSEs ranging from $0.097 \text{ to } 0.172 \text{ W m}^{-1} \text{ K}^{-1}$ and biases ranging from -0.053 to 0.053 W m^{-1} K⁻¹. Alternately, 0.5SC consistently underestimates λ_{sat} and the extent of underestimation increases with increasing λ_{sat} values. Overall, QC performs best among the four approaches benefiting from the availability of quartz content for all soils in the validation dataset. However, as stated previously, quartz contents and soil mineral composition information are usually not reported for soils, which typically limits the application of QC. DEM-GMM outperforms the other approaches that do not use measured quartz content as an input, with RMSE, bias and R^2 of 0.202 W m⁻¹ K⁻¹, 0.013 W m⁻¹ K⁻¹ and 0.89, respectively. The superior performance of DEM-GMM is particularly obvious in Group II where estimates using SC and 0.5SC significantly over- or under- estimate λ_{sat} values.

4.4. Estimate λ_s using the DEM-GMM approach

The new DEM-GMM approach provides accurate λ_{sat} estimates, which offers the possibility to estimate λ_{s} from porosity only. By combining Eqs. [4] and [11], the following expression can be obtained:

$$\left(\frac{\lambda_s}{\lambda_w}\right)^{1-\phi} = \phi^m \left(\frac{1 - \lambda_s / \lambda_w}{1 - \left(\lambda_s / \lambda_w\right)^{\phi}}\right)^m \tag{27}$$

With Eq. (27), one can estimate λ_s from porosity with the DEM-GMM approach using the fitted m values for each group reported in the previous section. Although it is impossible to determine the λ_s directly, we used indirect λ_s values estimated from measured λ_{sat} values (Eq. (24)) as benchmarks to evaluate the performance of the DEM-GMM approach and for comparisons with GMM (Eq. (6)) using QC, SC and 0.5SC to estimate λ_s for Soils 44–89 in the validation dataset. In Fig. 7 the general performance order of the four approaches is: QC > DEM-GMM > SC > 0.5SC. The performances of QC and DEM-GMM are similar, their RMSEs range from 0.743 to 0.872 W m⁻¹ K⁻¹, and their bias values range from -0.016 and 0.000 W m⁻¹ K⁻¹. Such a robust performance indicates that when quartz content is unknown, the DEM-GMM approach provides reliable λ_s estimates, which can be used as inputs to several λ models, e. g., the widely-used de Vries (1963) model.

5. Conclusion

We developed a DEM-GMM approach to estimate $\lambda_{\rm sat}$ values from sand content and porosity using a combination of differential effective medium theory and the geometric mean method. The effective cementation exponent (m) is the only unknown DEM-GMM parameter. The 43 soils in the calibration dataset were divided into three textural groups based on sand content: Group I ($f_{\rm sand} < 0.4$), Group II ($0.4 < f_{\rm sand} < 1$)

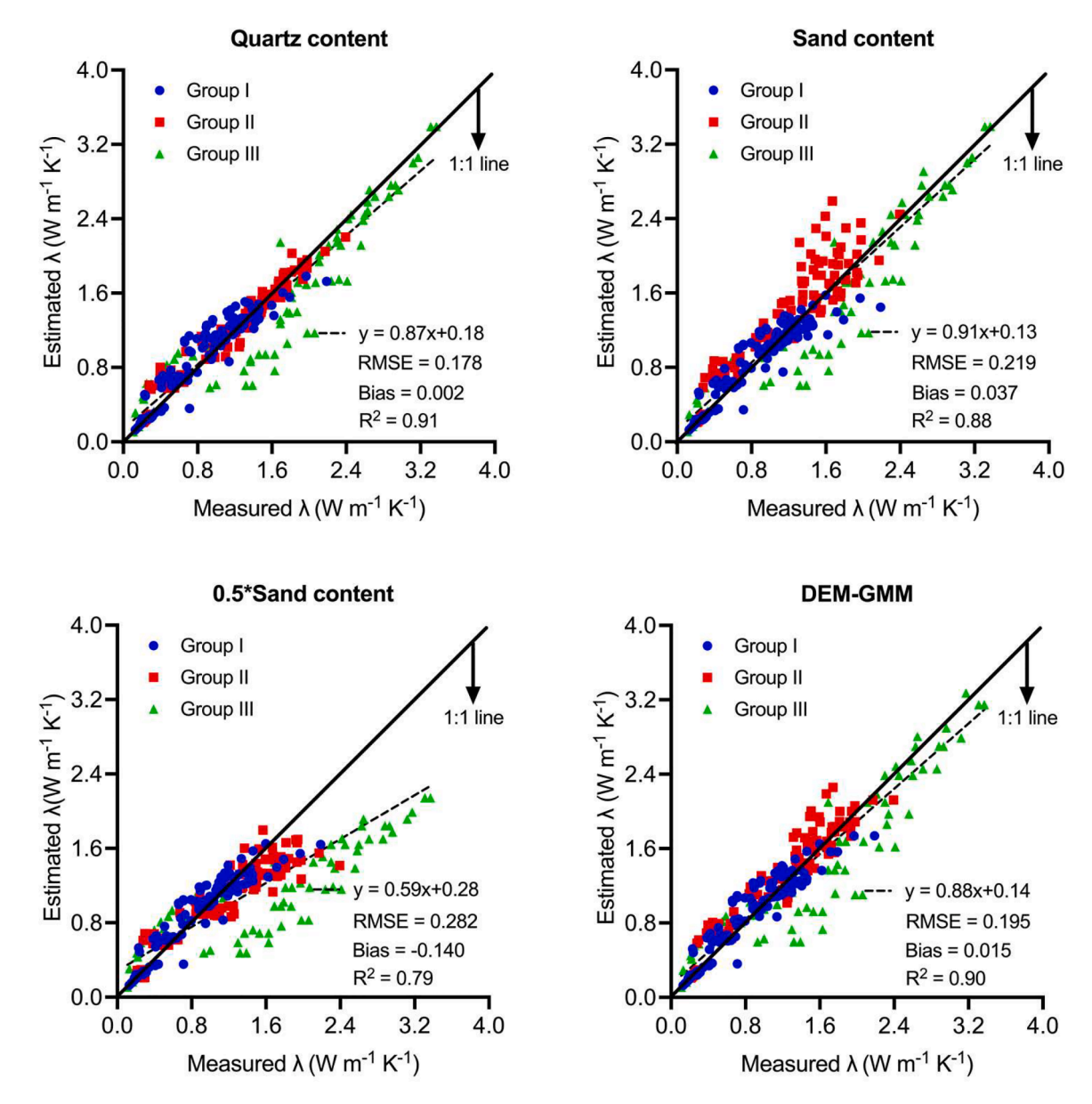


Fig. B.1. Comparison of λ values estimated with the Lu et al. (2007) model (Eq. (B.1)) where λ_{sat} is estimated with the geometric mean method (Eq. (7)) using either measured quartz content, or quartz content equal to sand content or to 0.5 \times sand content, and by the DEM-GMM approach (Eq. (25)) versus measured λ_{sat} for Soil 44-89 in the validation dataset. The solid lines are the 1:1 lines. Groups I, II and III represent soils with $f_{sand} < 0.4$, $0.4 \le f_{sand} < 1$ and $f_{sand} = 1$, respectively.

and Group III ($f_{\rm sand}=1$). The best-fitted values for m were 1.67 for Group I, 1.62 for Group II and -0.34 ϕ +1.70 for Group III. The DEM-GMM approach provided accurate $\lambda_{\rm sat}$ and $\lambda_{\rm s}$ estimates for another 46 soils when quartz content was not known. Once incorporated into existing thermal conductivity models, this can be further applied in more scenarios in the future.

Declaration of Competing Interest

The authors declare that they have no known competing financial interests or personal relationships that could have appeared to influence the work reported in this paper.

Data availability

Data will be made available on request.

Acknowledgments

This research was supported by the US National Science Foundation (Grant Number: 2037504) and USDA-NIFA Multi-State Project 4188. The Python code for implementing the DEM-GMM approach is available on HydroShare: http://www.hydroshare.org/resource/c69baedadad14b9ea4998769709fd16d.

Appendix A. Physical constraint on the cementation exponent m in the DEM-GMM approach

Eq. (20) can be rearranged as,

$$m > \frac{1}{1 - \left[\frac{d\phi_s\left(\frac{\lambda_s}{\lambda_w} - 1\right)}{\left(\frac{\lambda_s}{\lambda_w}\right) - 1} - 1\right] / \left(\frac{\lambda_s}{\lambda_w} - 1\right)} \tag{A.1}$$

For an infinitesimal increment of soil solids, dφ₅, the right side of Eq. [A.1] can be rewritten by applying L'Hôpital's rule,

$$\frac{\lim_{d\phi_{s}\to 0} \frac{1}{1 - \left[\frac{d\phi_{s}\left(\frac{\lambda_{s}}{\lambda_{w}}-1\right)}{\left(\frac{\lambda_{s}}{\lambda_{w}}\right)^{2}-1}\right] / \left(\frac{\lambda_{s}}{\lambda_{w}}-1\right)} = \frac{1}{1 - \left[\frac{\left(\frac{\lambda_{s}}{\lambda_{w}}-1\right)}{\ln\left(\frac{\lambda_{s}}{\lambda_{w}}\right)}-1\right] / \left(\frac{\lambda_{s}}{\lambda_{w}}-1\right)}$$
(A.2)

Then the inequality in Eq. [21] is obtained,

$$m > \frac{1}{1 - \left\lceil \frac{\left(\frac{\lambda_n}{\lambda_w} - 1\right)}{\ln\left(\frac{\lambda_n}{\lambda_w}\right)} - 1 \right\rceil / \left(\frac{\lambda_n}{\lambda_w} - 1\right)}$$
(A.3)

Combining Eqs. [24] and [A.3] yields,

$$m > \frac{1}{1 - \left\lceil \frac{\left(\left(\frac{\hat{\lambda}_{\text{sat}}}{\hat{\lambda}_{\text{w}}} \right)^{\frac{1}{1 - \phi}} - 1}{\frac{1}{1 - \phi} \ln \left(\frac{\hat{\lambda}_{\text{sat}}}{\hat{\lambda}_{\text{w}}} \right)^{-1}} - 1 \right\rceil} / \left\lceil \left(\frac{\hat{\lambda}_{\text{sat}}}{\hat{\lambda}_{\text{w}}} \right)^{\frac{1}{1 - \phi}} - 1 \right\rceil$$
(A.4)

While fitting the DEM-GMM approach (Eq. (25)) to the measured λ_{sat} (ϕ) values, we used Eq. (A.4) as the lower bound to obtain parameter m values for the 43 soils in the calibration dataset. As shown in Fig. A.1, none of the values reached the lower constraints during fitting, which, in turn, justifies that our derivation from DEM to GMM is robust.

Appendix B. Application: Incorporating the DEM-GMM approach into $\lambda(\theta)$ models

As stated earlier in Eq. (2a), any errors in λ_{sat} estimation will further lead to changes in λ of unsaturated soils. Thus, here we took the Lu et al. (2007) model as an example to investigate the performance of the DEM-GMM approach when incorporating into a $\lambda(\theta)$ model for soils 44–89 in the validation dataset. Lu et al. (2007) described K_e as an exponential equation of θ based on twelve soils:

$$K_{\rm e} = \frac{\lambda - \lambda_{\rm dry}}{\lambda_{\rm sat} - \lambda_{\rm dry}} = \exp\left\{\alpha \left[1 - \left(\frac{\theta}{\phi}\right)^{(\alpha - 1.33)}\right]\right\}$$
(B.1)

where λ_{dry} is the thermal conductivity of dry soil, α is a soil texture dependent parameter (i.e., 0.96 for coarse-textured soils with sand fraction (f_{sand}) \geq 0.4 and 0.27 for fine-textured soils with f_{sand} < 0.4) and 1.33 is a shape factor. Subsequently, λ_{sat} in Eq. (B1] is estimated with the DEM-GMM approach, and the GMM (Eq. (5)) using QC, SC or 0.5SC. For a fair comparison, we use the measured λ_{dry} values for all cases. The λ estimations presented in Fig. B.1 show similar trends as those reported for λ_{sat} : QC performs best with a lowest RMSE of 0.178 W m⁻¹ K⁻¹ and a bias closest to zero (i.e., 0.002 W m⁻¹ K⁻¹); the DEM-GMM performs second best with a slightly greater RMSE of 0.195 W m⁻¹ K⁻¹ and bias of 0.015 W m⁻¹ K⁻¹; followed by SC, and 0.5SC is the worst among the four approaches. Our results are consistent with He et al. (2020a) who also found that using the quartz content can improve the performances of all normalized $\lambda(\theta)$ models. However, when quartz content is unavailable, the DEM-GMM approach developed in this study, which only requires soil porosity, can be used to accurately estimate λ_{sat} and λ from $\lambda(\theta)$ models.

References

Archie, G.E., 1942. The electrical resistivity log as an aid in determining some reservoir characteristics. Trans. Aime 146, 54–62.

Barry-Macaulay, D., Bouazza, A., Wang, B., Singh, R.M., 2015. Evaluation of soil thermal conductivity models. Can. Geotech. J. 52, 1892–1900.

Bristow, K.L., 1998. Measurement of thermal properties and water content of unsaturated sandy soil using dual-probe heat-pulse probes. Agric. For. Meteorol. 89,

Bristow, K., Dane, J.H., Topp, G.C., 2002. Thermal conductivity. Methods of soil analysis:
Physical methods. Soil Science Society of America, Madison, WI, pp. 1209–1226.

Bussian, A.E., 1983. Electrical conductance in a porous medium. Geophysics 48, 1258–1268.

Côté, J., Konrad, J.M., 2005. A generalized thermal conductivity model for soils and construction materials. Can. Geotech. J. 42, 443–458.

Côté, J., Konrad, J.M., 2007. Indirect methods to assess the solid particle thermal conductivity of Quebec marine clays. Can. Geotech. J. 44, 1117–1127.

Calvet, J.C., Fritz, N., Berne, C., Piguet, B., Maurel, W., Meurey, C., 2016. Deriving pedotransfer functions for soil quartz fraction in southern France from reverse modeling. Soil 2, 615–629.

Campbell, G.S., Jungbauer, J.D., Bidlake, W.R., Hungerford, R.D., 1994. Predicting the effect of temperature on soil thermal conductivity. Soil Sci. 158, 307–313.

Chen, S.X., 2008. Thermal conductivity of sands. Heat Mass Transf. 44, 1241–1246.
Cosenza, P., Guérin, R., Tabbagh, A., 2003. Relationship between thermal conductivity and water content of soils using numerical modelling. Eur. J. Soil Sci. 54, 581–588.

Cosenza, P., Ghorbani, A., Camerlynck, C., Rejiba, F., Guérin, R., Tabbagh, A., 2009. Effective medium theories for modelling the relationships between electromagnetic properties and hydrological variables in geomaterials: a review. Near Surf. Geophys.

de Vries, D.A., Van Wijk, W.R., 1963. Thermal properties of soils. Physics of Plant Environment. Amsterdam.

Deepagoda, T.K.K.C., Smits, K., Ramirez, J., Moldrup, P., 2016. Characterization of thermal, hydraulic, and gas diffusion properties in variably saturated sand grades. Vadose Zone J. 15, 1–11.

- Dixon, C., Sheng, W., Zhou, R., Horton, R., Jones, S.B., 2023. Thermal property standards using granular media with air-pluviation and heat pulse probe measurements. Agric. For. Meteorol. 330, 109303.
- Donazzi, F., Occhini, E., Seppi, A., 1979. Soil thermal and hydrological characteristics in designing underground cables. Proc. Inst. Electr. Eng. 126, 506.
- Ewen, J., Thomas, H.R., 1987. The thermal probe—a new method and its use on an unsaturated sand. Géotechnique 37, 91–105.
- Friedman, S.P., 2005. Soil properties influencing apparent electrical conductivity: a review. Comput. Electron. Agric. 46, 45–70.
- Fu, Y., Horton, R., Ren, T., Heitman, J.L., 2021a. A general form of Archie's model for estimating bulk soil electrical conductivity. J. Hydrol., 126160
- Fu, Y., Lu, S., Ren, T., Horton, R., Heitman, J.L., 2021b. Estimating soil water retention curves from soil thermal conductivity measurements. J. Hydrol., 127171
- Fu, Y., Ghanbarian, B., Horton, R., Heitman, J., 2023. Robust calibration and evaluation of a percolation-based effective-medium approximation model for thermal conductivity of unsaturated soils. Geoderma 438, 116631.
- Glover, P.W.J., Ransford, T.J., Auger, G., 2010. A simple method for solving the Bussian equation for electrical conduction in rocks. Solid Earth 1, 85–91.
- Glover, P., 2009. What is the cementation exponent? A new interpretation. Lead. Edge 28, 82–85.
- Hailemariam, H., Shrestha, D., Wuttke, F., Wagner, N., 2017. Thermal and dielectric behaviour of fine-grained soils. Environ. Geotech. 4, 79–93.
- Hao, X., Ball, B., Culley, J., Carter, M., Parkin, G., Carter, M.R., Gregorich, E.G., 2008. Soil density and porosity. Soil Sampling and Methods of Analysis, 2nd ed. CRC Press, Boca Raton, pp. 743–760.
- He, H., Zhao, Y., Dyck, M.F., Si, B., Jin, H., Lv, J., Wang, J., 2017. A modified normalized model for predicting effective soil thermal conductivity. Acta Geotech. 12, 1281–1300.
- He, H., Dyck, M.F., Horton, R., Ren, T., Bristow, K.L., Lv, J., Si, B., 2018. Development and application of the heat pulse method for soil physical measurements. Rev. Geophys. 56, 567–620.
- He, H., Noborio, K., Johansen, Ø., Dyck, M.F., Lv, J., 2020a. Normalized concept for modelling effective soil thermal conductivity from dryness to saturation. Eur. J. Soil Sci. 71, 27–43.
- He, H., Li, M., Dyck, M., Si, B., Wang, J., Lv, J., 2020b. Modelling of soil solid thermal conductivity. Int. Commun. Heat Mass 116, 104602.
- He, H., Flerchinger, G.N., Kojima, Y., He, D., Hardegree, S.P., Dyck, M.F., Horton, R., Wu, Q., Si, B., Lv, J., Wang, J., 2021. Evaluation of 14 frozen soil thermal conductivity models with observations and SHAW model simulations. Geoderma 403, 115207.
- Hopmans, J.W., Dane, J.H., 1986. Thermal conductivity of two porous media as a function of water content, temperature, and density. Soil Sci. 142, 187–195.
- Horai, K., 1971. Thermal conductivity of rock-forming minerals. J. Geophys. Res. 76, 1278–1308.
- Hu, G., Zhao, L., Wu, X., Li, R., Wu, T., Xie, C., Pang, Q., Zou, D., 2017. Comparison of the thermal conductivity parameterizations for a freeze-thaw algorithm with a multilayered soil in permafrost regions. Catena 156, 244–251.
- Johansen, O., 1975. Thermal conductivity of soils. Ph.D. diss. Nor. Univ. Sci. Technol. Trondheim (CRRFL draft transl. 637, 1977)
- Trondheim (CRREL draft transl. 637, 1977).

 Jones, S.B., Friedman, S.P., 2000. Particle shape effects on the effective permittivity of anisotropic or isotropic media consisting of aligned or randomly oriented ellipsoidal particles. Water Resour. Res. 36, 2821–2833.
- Jougnot, D., Revil, A., 2010. Thermal conductivity of unsaturated clay-rocks. Hydrol. Earth Syst. Sci. 14, 91–98.
- Kasubuchi, T., Momose, T., Tsuchiya, F., Tarnawski, V., 2007. Normalized thermal conductivity model for three Japanese soils. Trans. Jpn. Soc. Irrig. Drain. Rural Eng. 251, 53–57. https://doi.org/10.11408/jsidre2007.2007.529.
- Lesmes, D.P., Friedman, S.P., Rubin, Y., Hubbard, S.S., 2005. Relationships between the electrical and hydrogeological properties of rocks and soils. Hydrogeophysics. Water Science and Technology Library. Springer, Dor-drecht vol 50.
- Lichtenecker, K., 1924. Der elektrische Leitungswiderstand k\u00fcnstlicher und nat\u00fcrlicher aggregate. Phys. Z. 25, 225-233, 169-181,193-204.
- Lu, S., Ren, T., Gong, Y., Horton, R., 2007. An improved model for predicting soil thermal conductivity from water content at room temperature. Soil Sci. Soc. Am. J. 71, 8–14.

- Lu, S., Ren, T., Yu, Z., Horton, R., 2011. A method to estimate the water vapour enhancement factor in soil. Eur. J. Soil Sci. 62, 498–504.
- Lu, Y., Wang, Y., Ren, T., 2013. Using late time data improves the heat-pulse method for estimating soil thermal properties with the pulsed infinite line source theory. Vadose Zone J. 12, 1–9.
- Maxwell, J.C., 1873. A Treatise on Electricity and Magnetism. Clarendon press. Mendelson, K.S., Cohen, M.H., 1982. The effect of grain anisotropy on the electrical properties of sedimentary rocks. Geophysics 47, 257–263.
- Nikolaev, I.V., Leong, W.H., Rosen, M.A., 2013. Experimental investigation of soil thermal conductivity over a wide temperature range. Int. J. Thermophys. 34, 1110–1129.
- Niu, Q., Zhang, C., 2018. Physical explanation of archie's porosity exponent in granular materials: a process-based, pore-scale numerical study. Geophys. Res. Lett. 45, 1870–1877.
- Niu, Q., Revil, A., Saidian, M., 2016. Salinity dependence of the complex surface conductivity of the Portland sandstone complex surface conductivity. Geophysics 81, D125–D140
- Peters-Lidard, C.D., Blackburn, E., Liang, X., Wood, E.F., 1998. The effect of soil thermal conductivity parameterization on surface energy fluxes and temperatures. J. Atmos. Sci. 55, 1209–1224.
- Ramires, M.L.V., Castro, C.A.N.de, Nagasaka, Y., Nagashima, A., Assael, M.J., Wakeham, W.A., 1995. Standard reference data for the thermal conductivity of water. J. Phys. Chem. Ref. Data 24, 1377–1381.
- Revil, A., 2000. Thermal conductivity of unconsolidated sediments with geophysical applications. J. Geophys. Res. Solid Earth 105, 16749–16768.
- Robinson, D.A., Friedman, S.P., 2001. Effect of particle size distribution on the effective dielectric permittivity of saturated granular media. Water Resour. Res. 37, 33–40.
- Robinson, D.A., Friedman, S.P., 2005. Electrical conductivity and dielectric permittivity of sphere packings: measurements and modelling of cubic lattices, randomly packed monosize spheres and multi-size mixtures. Phys. A Stat. Mech. Appl. 358, 447–465.
- Sass, J.H., Lachenbruch, A.H., Munroe, R.J., 1971. Thermal conductivity of rocks from measurements on fragments and its application to heat-flow determinations. J. Geophys. Res. 76, 3391–3401.
- Schönenberger, J., Momose, T., Wagner, B., Leong, W.H., Tarnawski, V.R., 2012. Canadian field soils I. Mineral composition by XRD/XRF measurements. Int. J. Thermophys. 33, 342–362.
- Sen, P.N., Scala, C., Cohen, M.H., 1981. A self-similar model for sedimentary rocks with application to the dielectric constant of fused glass beads. Geophysics 46, 781–795.
- Sen, P.N., 1984. Grain shape effects on dielectric and electrical properties of rocks. Geophysics 49, P586–P587.
- Simpkin, R., 2010. Derivation of Lichtenecker's logarithmic mixture formula from Maxwell's equations. IEEE Trans. Microw. Theory Tech. 58, 545–550.
- Smits, K.M., Sakaki, T., Howington, S.E., Peters, J.F., Illangasekare, T.H., 2013. Temperature dependence of thermal properties of sands across a wide range of temperatures (30–70°C). Vadose Zone J. 12 vzj2012.0033.
- Tarnawski, V.R., McCombie, M.L., Leong, W.H., Wagner, B., Momose, T., Schönenberger, J., 2012. Canadian field soils II. Modeling of quartz occurrence. Int. J. Thermophys. 33, 843–863.
- Tarnawski, V.R., McCombie, M.L., Momose, T., Sakaguchi, I., Leong, W.H., 2013.
 Thermal conductivity of standard sands. Part III. Full range of saturation. Int. J.
 Thermophys. 34, 1130–1147.
- Tarnawski, V.R., Momose, T., Leong, W.H., 2015. Assessing the impact of quartz content on the prediction of soil thermal conductivity. Géotechnique 59, 331–338.
- Wang, J., He, H., Li, M., Dyck, M., Si, B., Lv, J., 2020. A review and evaluation of thermal conductivity models of saturated soils. Arch. Agron. Soil Sci. 67, 974–986.
- Woodside, W., Messmer, J.H., 1961. Thermal conductivity of porous media. I. unconsolidated sands. J. Appl. Phys. 32, 1688–1699.
- Zakri, T., Laurent, J.P., Vauclin, M., 1998. Theoretical evidence for `Lichtenecker's mixture formulae' based on the effective medium theory. J. Phys. D Appl. Phys. 31, 1590
- Zhao, H., Zeng, Y., Lv, S., Su, Z., 2018. Analysis of soil hydraulic and thermal properties for land surface modeling over the Tibetan plateau. Earth Syst. Sci. Data 10, 1031–1061